JOURNAL OF PHYSICAL ORGANIC CHEMISTRY
J. Phys. Org. Chem. 2000; **13:** 870–879

Influence of structure on the kinetics of assembly of cyclic dipeptides into supramolecular tapes

Tzy-Jiun M. Luo and G. Tayhas R. Palmore*

Division of Engineering, Brown University, Providence, Rhode Island 02912, USA

Received 5 June 2000; revised 25 August 2000; accepted 25 August 2000

ABSTRACT: Cyclic dipeptides with a variety of substituents assemble into supramolecular tapes, which can function as scaffolds to position co-crystallized guest molecules. To examine how molecular structure influences the kinetics of crystal growth, we compared the rate at which two cyclic dipeptides assembled into supramolecular tapes using atomic force microscopy as an *in situ* probe of the kinetics of step advancement in these crystalline solids. Changes in the molecular structure of the substituents from two hydrogen atoms on the cyclic dipeptide of glycine (GLYDKP) to two methyl groups on the cyclic dipeptide of alanine (*R*,*R*-ALADKP) reduces the rate at which *R*,*R*-ALADKP assembles into supramolecular tapes by a factor between four and five relative to that of GLYDKP. These results are discussed in the context of barriers to desolvation, surface diffusion, ledge diffusion and incorporation into kink sites and the energies of adsorption at these different sites on a crystal. We show that the difference in the rate at which these two molecules assemble into tapes corresponds to the difference in the barriers for attachment to a kink site at the temperature and concentrations used. The degree to which these solutes must change conformationally is proposed to be the source of the observed difference in the barriers for incorporation into a kink site. Copyright © 2000 John Wiley & Sons, Ltd.

KEYWORDS: atomic force microscopy; crystal engineering; cyclic dipeptides; hydrogen bonds; self-assembly

INTRODUCTION

The amide functional group has been used by researchers as an element for designing natural and non-natural supramolecular structures that self-assemble through hydrogen-bonding interactions. The majority of research has focused on designing supramolecular structures either in solution or in solids. Several reviews have appeared in the literature describing supramolecular structures that recognize specific substrates, self-replicate, show catalytic activity in solution[1–6] or function as scaffolds in solids (i.e. crystal engineering).[7–13] Since Schmidt first introduced the term 'crystal engineering' in 1971, research involving the design of supramolecular structures in solids has grown exponentially.[14] In addition to studying the self-assembly of amides in solution and in the solid state, a number of groups now are using amides to create supramolecular structures in liquid-crystalline media and at surfaces.[15,16] A common goal of many such studies on the assembly of molecules containing amides and other functional groups is the ability to create supramolecular structures with predetermined properties or function. Success in this area would have implications for many technologies that require the development of novel, complex materials to meet increasing demands for specificity and miniaturization.

The quality and size of most organic crystals are inadequate for material applications and therefore must be improved. Understanding the mechanism of self-assembly should enable us to produce crystalline solids of higher quality with predetermined properties. Accordingly, we have compared the rate at which two cyclic dipeptides assemble into supramolecular structures using atomic force microscopy as an *in situ* probe of the kinetics of step advancement in these crystalline solids. We show that changes in the molecular structure of the substituents from two hydrogen atoms on the cyclic dipeptide of glycine (GLYDKP) to two methyl groups on the cyclic dipeptide of alanine (*R*,*R*-ALADKP) reduces the rate at which *R*,*R*-ALADKP assembles into supramolecular structures by a factor between four and five relative to that of GLYDKP. We discuss these results in the context of barriers to desolvation, surface diffusion, ledge diffusion and incorporation into kink sites and the energy of binding at these different sites on a crystal. We show that the difference in the rate at which these two molecules assemble into supramolecular structures corresponds to the difference in the barriers

**Correspondence to:* G. T. R. Palmore, Division of Engineering, Brown University, Providence, Rhode Island 02912, USA.

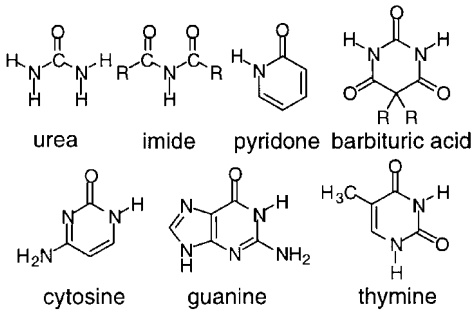

Figure 1. Examples of amides including some structures normally not classified as amides

for attachment to a kink site at the temperature and concentrations used. We propose that the difference in the barriers for incorporation into a kink site is due to conformational changes that must occur prior to incorporation of these solutes into their respective kink sites. By quantifying the influence of molecular structure on the kinetics of assembly, these findings contribute to the growing body of knowledge of materials design based on solvent-mediated assembly.

AMIDES AND THEIR PATTERNS OF HYDROGEN BONDING

A molecule can be considered an amide if it has a carbonyl group bonded directly to a nitrogen atom, regardless of whatever other atoms may be connected to the carbonyl group and nitrogen atom. This definition includes a range of structures that normally are not classified as amides (Fig. 1). Primary amides predominantly form the type of hydrogen-bonded structure shown in Fig. 2.[17] This structure contains two different types of hydrogen bonds that give a ring motif and a chain motif, which together form an infinite chain of rings.[18–20] Secondary amides simply form chains and tertiary amides do not form hydrogen bonds with themselves owning to the absence of a hydrogen bond donor (i.e. a hydrogen atom on a heteroatom).[21–25]

The geometry of the two hydrogen atoms on primary amides determines the type of structure that is formed through self-aggregation or by aggregation with a guest molecule. The orientation of these hydrogen atoms is defined as having either *syn* or *anti* geometry, depending on whether the hydrogen atom and the carbonyl group are located on the same side or the opposite side of the C— N bond (Fig. 3).[17] Hydrogen bonding between the *syn* hydrogen atom and the carbonyl group of two primary amides results in eight-membered rings, a motif analogous to the ring motif that forms between two carboxylic acids. The *anti* hydrogen atoms make single point contacts with carbonyl groups on neighboring amides to form chains. Since acyclic secondary amides prefer to adopt a conformation that places the amido hydrogen

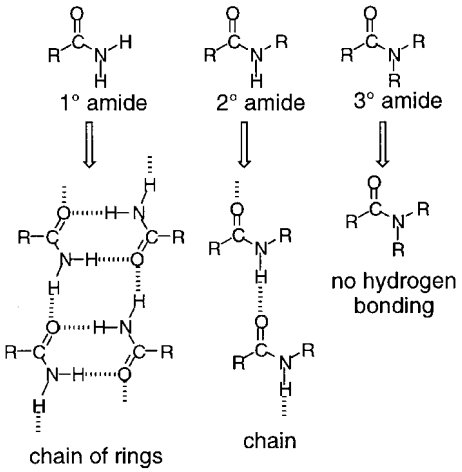

Figure 2. Patterns of hydrogen bonds formed by primary, secondary and tertiary amides

atom in the *anti* position, acyclic secondary amides generally form chains. Cyclic secondary diamides (e.g. cyclic dipeptides), in which the amido hydrogen atom is restricted to the *syn* position, generally form hydrogen-bonded rings, although other patterns of hydrogen bonds also are observed for these compounds.[10]

Several factors govern the types of supramolecular structures that result from the assembly of amides. These factors include the geometry of the amide, the number and type of substituents attached to the nitrogen atom, the number of different amides that are present in a molecule and the proximity of neighboring functional groups that may alter the hydrogen-bonding capacity of amides both sterically and electronically. With amides serving to link molecules via hydrogen bonds, a variety of supramolecular structures (Fig. 4) have been assembled that are described as capsules and spheres,[3,26,27] channels,[8,9,28,29] helices,[11,30] ribbons or tapes,[10,31–38] rods,[39] rosettes,[40,41] sheets or layers[17,28,29,36,42–52] and tubes.[16,53–55]

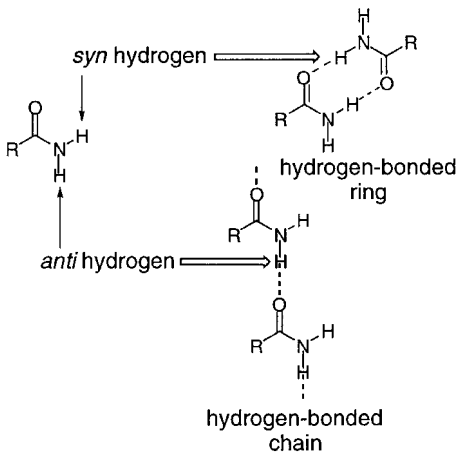

Figure 3. Ring and chain motifs generated by hydrogen-bonding interactions involving the *syn* and *anti* hydrogen atoms, respectively, of primary and secondary amides

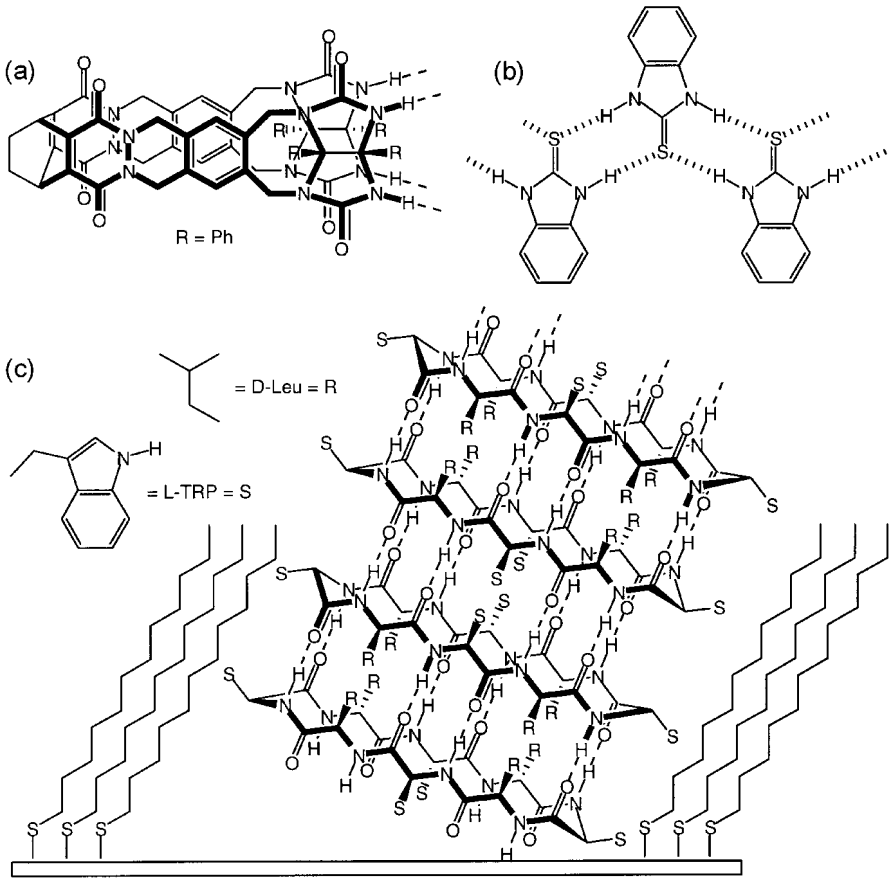

Figure 4. Three of many examples of supramolecular structures that assemble through hydrogen-bonding interactions between amides: (a) capsules,[26] (b) tapes[37] and (c) tubes[16]

SUPRAMOLECULAR TAPES

Our efforts have been focused on the self-assembly of diamides, specifically cyclic dipeptides. These compounds have a propensity to assemble into supramolecular tapes, a process driven predominantly by the formation of hydrogen bonds (N—H…O) between *cis*-amides on adjacent molecules (Fig. 5).[38] Our goal is to use supramolecular tapes as scaffolds with which to position guest molecules within the crystalline lattice for the purpose of creating a solid with tunable properties that depend on the arrangement and structure of the guest molecules. To achieve this goal requires the development of methods for predicting which guest molecules can be incorporated into a crystalline lattice of cyclic dipeptides and the development of methods for measuring how molecular structure influences the kinetics of assembly. Understanding what patterns of packing cyclic dipeptides can adopt should provide insight into how tapes comprised of cyclic dipeptides can be used to control the structure and function of co-crystalline solids.

It has been shown previously that symmetrically substituted cyclic dipeptides will assemble into tapes even when their substituents occupy volumes as large as 290 Å^3.[38] Despite the variability in volume and shape represented by these molecules, the persistence of the tape motif in their crystalline solids suggests that the hydrogen-bonding interactions between cyclic dipeptides (i.e. amide–amide interactions) dominate the packing arrangement of these molecules. Moreover, void space in these crystalline solids is minimized by the parallel alignment of tapes (Fig. 6). In a subsequent study, we demonstrated that the cyclic dipeptide of aspartic acid assembles into tapes possessing pendant carboxylic acid groups, which could be used to position guest molecules (i.e. those with good hydrogen-bond acceptors such as derivatives of pyridine) at well-defined intervals along the backbone of tapes (Fig. 7).[42,56]

Depending on the molecular structure of the guest,

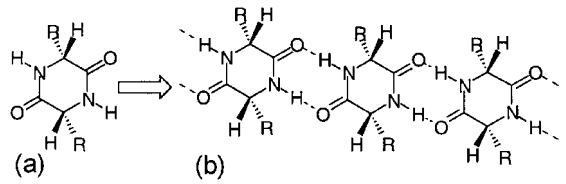

Figure 5. (a) Molecular structure of GLYDKP (R=H) or *R,R*-ALADKP (R=CH_3). (b) Hydrogen-bonded tape that results when *cis*-amides on adjacent molecules interact in an $R_2^2(8)$ pattern of hydrogen bonds

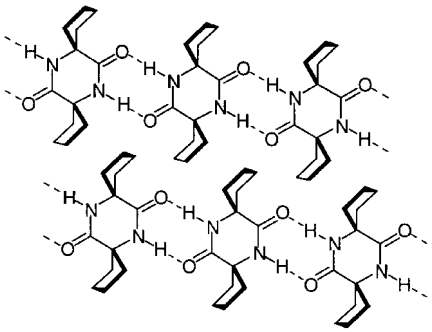

Figure 6. One of eight symmetrically substituted cyclic dipeptides (spirocyclopentyl-2,5-diketopiperazine) that self-assemble into hydrogen-bonded tapes[38]

tapes can be cross-linked into layers or simply used to align guests on adjacent tapes. The ability to interchange one guest molecule for another provides a powerful and convenient method for manipulating the physical properties of these crystalline materials without significantly altering the framework of tapes that define the supramolecular structure within the crystalline lattice.

MORPHOLOGY OF CRYSTALS WITH SUPRAMOLECULAR TAPES

In addition to modeling and crystallographic studies, we have used atomic force microscopy (AFM) to measure the rates at which cyclic dipeptides assemble into tapes.[57]

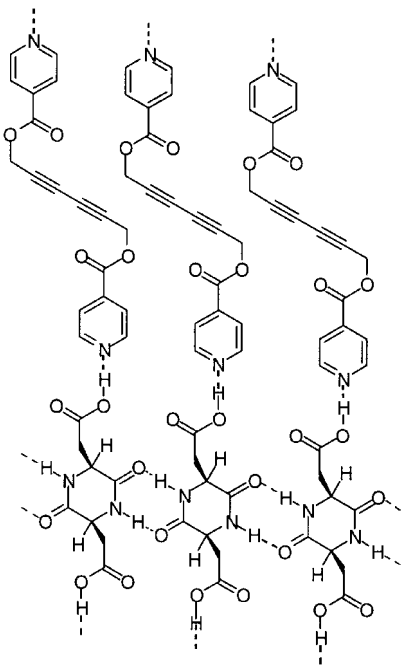

Figure 7. The cyclic dipeptide of *S*-aspartic acid (*S,S*-ASPDKP) assembles into hydrogen-bonded tapes, which function as scaffolds for positioning guest molecules such as derivatives of bis-pyridine[56]

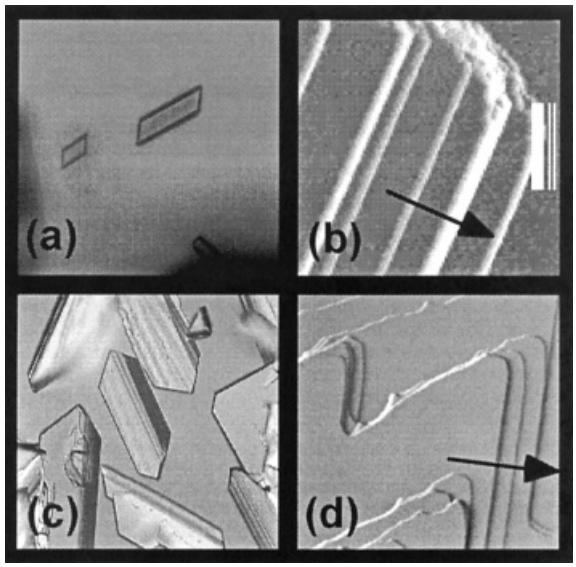

Figure 8. Colorless crystals ($\sim 2 \times 1 \times 0.1$ mm) of (a) GLYDKP and (c) *R,R*-ALADKP grown from aqueous solutions and their respective AFM images (b) (3×3 μm) and (d) (5×5 μm). The large terraces (gray) in the AFM images correspond to hydrophobic $\rangle CH_2$ groups of GLYDKP (010 crystal plane) or $\rangle CHCH_3$ groups of *R,R*-ALADKP (001 crystal plane). The long axes of the tapes in both crystals correspond to the smooth step edges in the AFM images. Thus, step risers for the smooth step edges correspond to the plane of the DKP rings and step risers for the rough step edges correspond to amide groups at the ends of tapes. The arrows in (b) and (d) indicate the direction of step advancement for which velocity as a function of supersaturation was measured

We (and others) have studied how the rate of growth of a crystal depends on molecular structure or environmental factors such as chemical additives.[57–59] Reported here are results from our AFM studies on the self-assembly of the cyclic dipeptides of glycine (GLYDKP) and alanine (ALADKP), which illustrate how both surface morphology and the kinetics of assembly correlate with the anisotropy of the intermolecular interactions as well as molecular asymmetry.

Thin plates $1.0 \times 1.0 \times 0.2$ cm in size result when crystals of GLYDKP are grown from an aqueous solution containing this compound [Fig. 8(a)]. The largest, and therefore slowest, growing surface on a crystal of GLYDKP grown from an aqueous solution is comprised of protruding —CH_2 groups and oxygen atoms from one of the two carbonyl groups of GLYDKP. This relatively non-polar surface is the consequence of GLYDKP assembling into tapes that pack with their long axes in parallel to form decks of tapes. The large terraces (010 plane) in the AFM image (3×3 μm) of a crystal of GLYDKP correspond to this non-polar surface [Fig. 8(b)]. The terraces are delineated by step edges with morphologies that are either smooth or rough. The x-ray

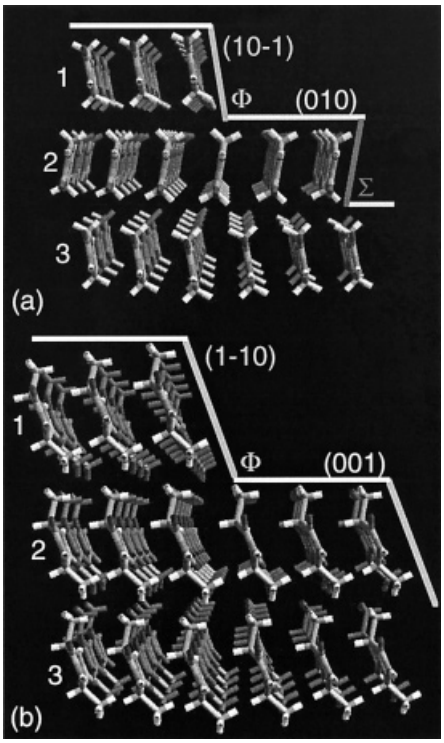

Figure 9. View looking down the long axes of tapes in the crystal structures of (a) GLYDKP and (b) *R,R*-ALADKP. Three decks of tapes are shown for each crystal structure. The angles between the (010) terraces and the (10–1) step risers in GLYDKP are obtuse (ϕ) or acute ($\sum$) and reflect the twofold screw axis of symmetry in the crystal structure of GLYDKP ($P2_1/c$). The crystal structure of *R,R*-ALADKP is noncentrosymmetric ($P1$) and, therefore, angles (ϕ) between the (001) terraces and the (1–10) step risers on the crystal face shown are equivalent and obtuse

crystal structure of GLYDKP shown in Fig. 9(a) depicts the chemical composition of the different surfaces of a crystal of GLYDKP.[60] In addition to the (010) terraces, the step risers (one molecule in height = 5.8 Å) of the smooth (10–1) and rough (100 and 001) step edges comprise DKP rings and amide groups at the ends of tapes, respectively.

Replacing one of the two hydrogen atoms at both the 1- and 4-positions of GLYDKP with a methyl group gives the cyclic dipeptide of alanine (ALADKP). In addition to an increase in the specific molecular volume (174.76 Å^3 for ALADKP vs 115.94 Å^3 for GLYDKP), this replacement generates two stereocenters in the molecular structure of ALADKP. The result is three possible stereoconfigurations: *R,R*-ALADKP, *S,S*-ALADKP and *R,S*-ALADKP. The studies described here were conducted on the *R,R*-stereoisomer of ALADKP. Similarly to GLYDKP, molecules of *R,R*-ALADKP assemble into tapes that pack with their long axes in parallel to form decks of tapes. Thus, crystals of *R,R*-ALADKP also grow as thin plates [Fig. 8(c)] from an aqueous solution of this compound with the largest surface comprised of protruding $\diagdown\!\!\diagup$CH(CH_3) groups. Imaged with an AFM, this surface appears as large terraces (001 plane) delineated by step edges with morphologies that are either smooth or rough [Fig. 8(d)]. The x-ray crystal structure of *R,R*-ALADKP shown in Fig. 9(b) depicts the chemical composition of the different surfaces of a crystal of *R,R*-ALADKP.[61] In addition to the (001) terraces, the step risers (one molecule in height = 7.5 Å) of the smooth (1–10) and rough (100 and 010) step edges comprise DKP rings and amide groups at the ends of tapes, respectively.

KINETIC THEORY OF CRYSTAL GROWTH

From Burton–Cabrera–Frank theory of crystal growth, three types of diffusion contribute to the growth of a crystal at step edges: exchange of molecules between bulk solution and the adsorption layer at the surface of the crystal, exchange of molecules between the adsorption layer and step edges and exchange of molecules between step edges and kink sites.[62] The relationship between the velocity at which a step edge advances and supersaturation is given by

$$v_\infty = \beta\Omega C^\circ\sigma\frac{1}{1+\left(\frac{\beta h}{\pi D}\right)\left[\ln\left(\frac{d\pi}{h}\right)\right]} \qquad (1)$$

where β is the kinetic coefficient for step integration, Ω is the specific molecular volume, C° is the equilibrium concentration, σ is supersaturation, h is the height of the step, D is the diffusion coefficient and d is the distance from the step where solute concentration is equal to that of the bulk. The kinetic coefficient for step integration is given by

$$\beta = \frac{h^2\nu}{\delta_0}e^{\frac{-\Sigma G^\ddagger}{kT}} \qquad (2)$$

where ν is a frequency factor (e.g. $\sim 10^{18}$ s^{-1} for naphthalene), δ_0 is the thickness of the diffusion layer and $\Sigma G\ddagger$ is the sum of the energy barriers for dehydration, surface diffusion, ledge diffusion and incorporation at a kink site of a growth unit [Fig. 10(a)]. Depending on whether crystal growth is controlled by kinetics [$h^{-1}\pi D \gg \beta$, Fig. 10(b)] or diffusion [$h^{-1}\pi D \ll \beta$, Fig. 10(c)], Eqn. (1) simplifies to Eqn. (3) or (4), respectively:[63]

$$v_\infty = \beta\Omega C^\circ\sigma = \beta\Omega(C - C^\circ) \qquad (3)$$

$$v_\infty = \pi D\Omega C^\circ\sigma\frac{1}{h\ln\left(\frac{d\pi}{h}\right)} = \pi D\Omega(C - C^\circ)\frac{1}{h\ln\left(\frac{d\pi}{h}\right)} \qquad (4)$$

Results from the experiments reported here were

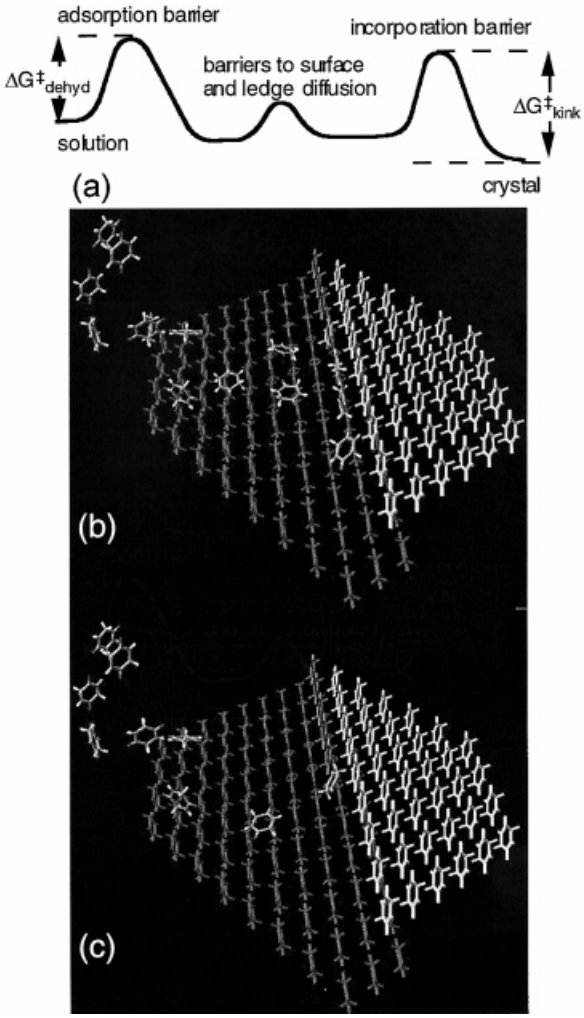

Figure 10. (a) The energy barriers to growth of a crystal from a supersaturated solution where $\Delta G\ddagger_{1,\text{dehyd}}$ and $\Delta G\ddagger_{\text{kink}}$ refer to the energy required to dehydrate one side of the solute and to incorporate it into a kink site, respectively. Crystal growth controlled by (b) kinetics ($h^{-1}\pi D \gg \beta$) or (c) diffusion ($h^{-1}\pi D \ll \beta$)

obtained by measuring the velocity of step advancement under conditions of kinetic limited growth. Equation (3) was used to calculate the kinetic coefficient for advancement of the smooth step edges in crystals of GLYDKP and *R,R*-ALADKP. The influence of molecular structure on the kinetics of self-assembly can be quantified by comparing the values of β obtained for these step edges.

KINETICS OF ASSEMBLY OF SUPRAMOLECULAR TAPES

The smooth step edges of GLYDKP (i.e. defined by the intersection of the (010) and (10–1) crystal planes) advance at velocities that depend linearly on the supersaturation of the growth solution (Fig. 11). Supersaturation, defined by $\sigma = (C/C^\circ) - 1$, where C and C° are the actual and equilibrium concentrations of GLYDKP, respectively, was varied from 0.067 to 0.253 by adjusting the concentration of GLYDKP. At these supersaturations, only doubled steps (i.e. two molecules in height where $h = 11.6$ Å) of GLYDKP were observed with the AFM. The doubling of steps is due to the symmetry of the crystal.[64] For example, the presence of a glide plane in the crystalline structure of GLYDKP manifests as tapes canted relative to the *b*-axis, creating either an acute (Σ) or obtuse (Φ) angle between a step riser and the adjoining terrace in the *a,c*-plane [Fig. 9(a)]. The attachment of molecules of solute to a step edge will be facilitated or hindered by the angle encountered and thus, molecules of solute attach to step edges comprised of step risers with acute or obtuse angles relative to the adjoining terrace at slightly different rates. Consequently, the step edge of one of two adjacent crystal layers will advance at a rate that is slightly slower than the step edge of the other crystal layer. The result is a doubled step with the rate of advancement limited by the slow step edge in the lower of the two crystal layers.

The velocities of step advancement for the smooth step edges of GLYDKP (intersection of the 010 terrace with the 10–1 step riser) and *R,R*-ALADKP (intersection of the 001 terrace with the 1–10 step riser) as a function of supersaturation are plotted in Fig. 11. Each data point for GLYDKP in Fig. 11 represents the average rate at which doubled steps advance at a given supersaturation, whereas each data point for *R,R*-ALADKP represents the average rate at which single steps advance at a given supersaturation. From Fig. 11 and Eqn. (3), the kinetic coefficient (β_1) for the smooth step edges of GLYDKP is calculated to be 17.1×10^{-3} cm s^{-1} using a value extrapolated from the velocity data of 0.149 M for C°

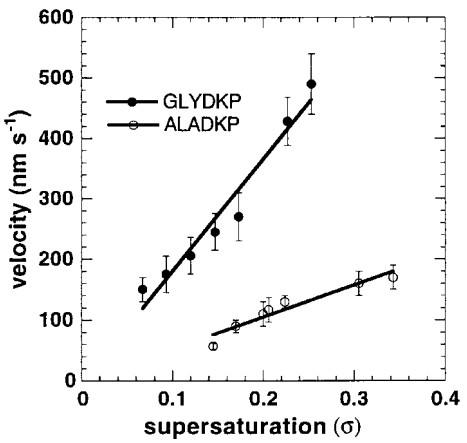

Figure 11. Growth kinetics of the smooth step edge (intersection of 010 terrace with 10–1 step riser) of GLYDKP compared with that of the smooth step edge (intersection of 001 terrace with 1–10 step riser) of *R,R*-ALADKP. Velocities of step advancement were measured at 25.0 °C and are linear with supersaturation. Supersaturation was adjusted by varying the concentration of GLYDKP (0.160–0.188 M) and *R,R*-ALADKP (0.189–0.220 M)

of GLYDKP. Recall from Eqn. (2) that β is related to the sum of the energy barriers for dehydration, surface diffusion, ledge diffusion and incorporation of a growth unit at a kink site. Thus, the value obtained for β will vary with the solid studied. When the rate of assembly of *R,R*-ALADKP is compared with that of GLYDKP, we find that the slightly larger, chiral molecules of *R,R*-ALADKP assemble into tapes more slowly than the smaller, achiral molecules of GLYDKP. In fact, at identical supersaturation, the relative rates at which the smooth step edges of GLYDKP and *R,R*-ALADKP advance typically range between 4:1 to 5:1. From Fig. 11 and Eqn. (3), where the equilibrium concentration of *R,R*-ALADKP extrapolated from the velocity data is 0.168 M, β_2 for the smooth step edge of *R,R*-ALADKP is calculated to be 3.5×10^{-3} cm s^{-1}, approximately one quarter the value of β_1 for the smooth step edges of GLYDKP.

The fourfold difference in the values for β for GLYDKP and *R,R*-ALADKP is a consequence of differences in their respective energy barriers for dehydration, surface diffusion, ledge diffusion and incorporation of a growth unit at a kink site. Although the energy barriers for dehydration and incorporation of a growth unit at a kink site typically are rate limiting when a crystal is grown under kinetic control, it is instructive to consider how structurally related growth units can differ in terms of energy barriers for surface and ledge diffusion. Figure 12(a) illustrates how the interactions between a chiral molecule such as *R,R*-ALADKP and a crystal terrace or ledge will differ based on the relative orientation of the molecule to the surface or ledge. For example, molecules labeled **Sa** and **Sb** in Fig. 12(a) reflect whether the methyl groups of *R,R*-ALADKP are oriented toward or away from the surface of the crystal, respectively.

The average energy of adsorption of molecules **Sa** or **Sb** can be calculated using the MINIMIZER module of Cerius[2] (version 3.8) parameterized with the Drieding force field. We define the energy of adsorption as the sum of all interactions between the surface of the crystal and a single molecule in the absence of solvent and define the average energy of adsorption as the average value obtained from several computational experiments. Initially, a single molecule of GLYDKP or *R,R*-ALADKP was sketched using the 3-D Builder in Cerius[2]. Equilibrium charges were calculated prior to minimization using the QEq 1.1 parameter set with a convergence criterion of 5.0×10^{-4}.[65] The molecule was minimized using the Newton Raphson method with the CVFF95 force field. Convergence criteria were 0.1 kcal mol^{-1} Å^{-1} (1 kcal = 4.184 kJ) for the r.m.s. with a maximum displacement of 2.0 Å. Convergence was obtained typically within 500 iterations. Once the molecule had been minimized, it was treated as a rigid body and placed in contact with its corresponding crystal surface (i.e. 010 for GLYDKP, 001 for *R,R*-ALADKP) comprised of a 10×10 array of molecules built from single-crystal x-ray data. The location and orientation of a single molecule were varied relative to the crystal surface. The energies of the resulting structures subsequently were minimized and averaged to give the average energy of adsorption.

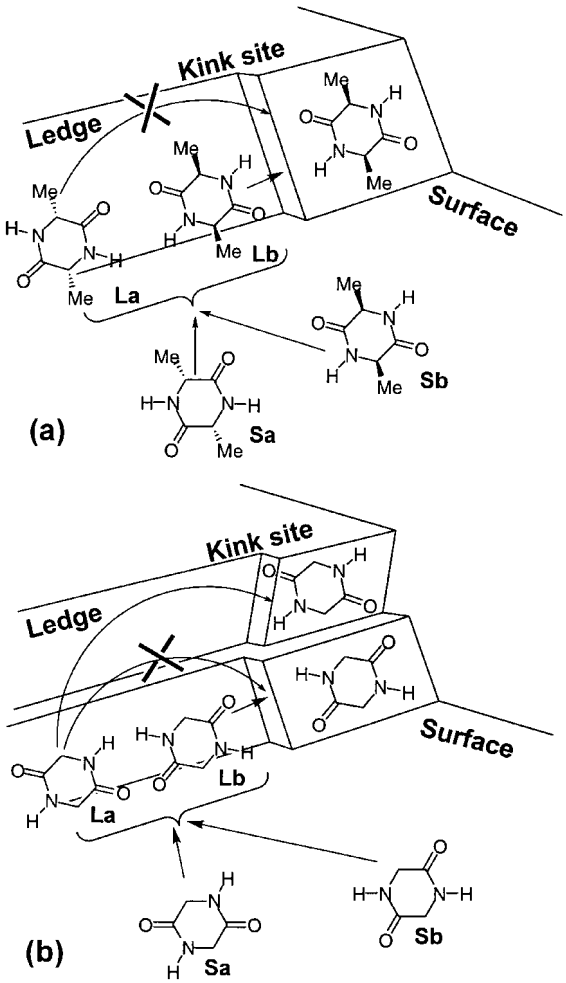

Figure 12. Different orientations of molecules of (a) *R,R*-ALADKP and (b) GLYDKP relative to their respective crystal surfaces and ledges

The difference in the average energies of adsorption of molecules of *R,R*-ALADKP labeled **Sa** and **Sb** in Fig. 12a is calculated to be 0.5 kcal mol^{-1}. Consequently, if the difference in energy barriers for surface diffusion follow the trend observed for the difference in the average energies of adsorption, **Sa** and **Sb** should diffuse toward a ledge or kink site at different rates. A similar argument holds for the rates at which molecules labeled **La** and **Lb** should diffuse along a ledge to a kink site. Unlike *R,R*-ALADKP, the orientation of achiral molecules of GLYDKP on the surface (**Sa** vs **Sb**) of a GLYDKP crystal [Fig. 12(b)] are indistinguishable in terms of their average energy of adsorption and energy barriers to surface diffusion. Therefore, we would expect their rates of surface diffusion to be equivalent. Similarly, the average energy of adsorption of molecules of

GLYDKP along the ledge (**La** vs **Lb**) of a GLYDKP crystal are expected to be equivalent.

It is interesting that in addition to differences in the average energy of adsorption of chiral molecules oriented differently on the surface or ledge of a crystal, there is a statistical difference to their incorporation into a chiral kink site compared with achiral molecules. For example, assuming equal concentrations of **La** and **Lb** exist at any given moment in time, only half of the molecules of *R,R*-ALADKP adsorbed on the ledge depicted in Fig. 12(a) would have the correct orientation for incorporation at the kink site (e.g. **Lb** but not **La**). Owing to the arrangement of the hydrogen-bond donors and acceptors in cyclic dipeptides, the same statistical difference is present when a growth unit is comprised of dimers or oligomers because all of the methyl substituents of *R,R*-ALADKP would be oriented in the same direction. In contrast, both **La** and **Lb** molecules of GLYDKP positioned at the prochiral ledges in Fig. 12(b) have the correct orientation for incorporation at these kink sites. Thus, molecules of GLYDKP oriented in the manner of **La** and **Lb** contribute to the advancement of the doubled step edge depicted in Fig. 12(b) whereas only molecules of *R,R*-ALADKP oriented in the manner **Lb** contribute to the advancement of the step edge depicted in Fig. 12(a). It could be argued that the flux of molecules of *R,R*-ALADKP to kink sites compared with that of molecules of GLYDKP is lower because of the statistical difference in the number of molecules that can be incorporated into a kink site and thus, this difference in flux could reduce β_2 for *R,R*-ALADKP by as much as half the value of β_1 for GLYDKP. A reduction in β due to this statistical difference, however, is not observable because the interconversion of **La** and **Lb** is not rate limiting.

BARRIERS TO ASSEMBLY

The difference in the sum of the energy barriers for dehydration, surface diffusion, ledge diffusion and incorporation of a growth unit at a kink site for GLYDKP ($\Sigma G\ddagger_1$) and *R,R*-ALADKP ($\Sigma G\ddagger_2$) can be determined from the equation

$$\frac{\beta_2}{\beta_1} = \frac{\frac{{h_2}^2 \nu}{\delta_0} e^{\frac{-\Sigma G_2^{\ddagger}}{kT}}}{\frac{{h_1}^2 \nu}{\delta_0} e^{\frac{-\Sigma G_1^{\ddagger}}{kT}}} \qquad (5)$$

Here the step heights (h_1 and h_2) for GLYDKP and *R,R*-ALADKP are 5.8 Å (single step) and 7.5 Å, respectively, and the remaining variables are as defined above.

The advancement of step edges, and thus β, was measured under conditions where crystal growth was controlled by kinetics ($h^{-1}\pi D \gg \beta$). Consequently, the energy barriers to surface and ledge diffusion are small relative to the energy barriers for dehydration and incorporation of a growth unit at a kink site and, therefore, not rate limiting. The values for the energy of hydration for GLYDKP and *R,R*-ALADKP are reported to be -18.5 and -17.8 kcal mol^{-1}, respectively.[66] Based on the Hammond postulate, we expect the barriers to dehydration of these two compounds also to be similar and, thus, this component of $\Sigma G\ddagger$ will cancel in Eqn. (5). These two points taken together suggest that ($\Sigma G\ddagger_2 - \Sigma G\ddagger_1$) in Eqn. (5) can be taken to represent the difference in energy barriers for incorporation of a growth unit at a kink site ($\Delta G\ddagger_{2,\mathrm{kink}} - \Delta G\ddagger_{1,\mathrm{kink}}$) in the equation

$$\Sigma G^{\ddagger}_2 - \Sigma G^{\ddagger}_1 \approx \Delta G^{\ddagger}_{2,kink} - \Delta G^{\ddagger}_{1,kink} \qquad (6)$$

Thus, by rearranging Eqn. (5) and applying the approximation given in Eqn. (6), $\Delta G\ddagger_{2,\mathrm{kink}}$ for *R,R*-ALADKP is calculated to be 1.24 kcal mol^{-1} higher than $\Delta G\ddagger_{1,\mathrm{kink}}$ for GLYDKP.

The conformations of GLYDKP and *R,R*-ALADKP in the solid state were compared with their conformation in the gas phase in an attempt to understand what factors might contribute to the 1.24 kcal mol^{-1} difference in energy barriers for incorporation of these molecules at a kink site with the assumption that the gas phase and solution phase conformations are similar. Molecules of *R,R*-ALADKP and GLYDKP were minimized using the same method described above. We found that the angles α and γ of *R,R*-ALADKP must undergo changes that are greater than those of GLYDKP when going from the conformation calculated in the gas phase to the conformation observed in the solid state (Table 1). The conformation of *R,R*-ALADKP in the gas phase exhibits a slightly puckered DKP ring whereas GLYDKP is planar (Fig. 13). A small amount of pucker in the DKP ring decreases steric interactions between the DKP ring and the two methyl substituents of *R,R*-ALADKP and also reduces ring strain in the DKP ring. For *R,R*-ALADKP to become incorporated into a kink site, angles α and γ must decrease by 12.7° and 32.5°, respectively. These changes in α and γ cause the DKP ring to become more puckered and, thus, more strained than the gas-phase conformation of the DKP ring in *R,R*-ALADKP. Any change in α and γ that increases ring strain will increase the energy barrier for incorporation into a kink site. This increase in ring strain is greater for *R,R*-ALADKP than for GLYDKP since α and γ for the gas-phase conformation of GLYDKP remain unchanged in the solid-phase conformation of GLYDKP (Table 1).

Figure 14 depicts the changes in energy that occur during the crystallization of GLYDKP and *R,R*-ALADKP. The difference in free energy between a molecule in solution and its corresponding crystalline state has been reported to be -2.3 and -2.7 kcal mol^{-1} for *R,R*-ALADKP and GLYDKP, respectively.[67] Since both cyclic dipeptides are reported to have similar values

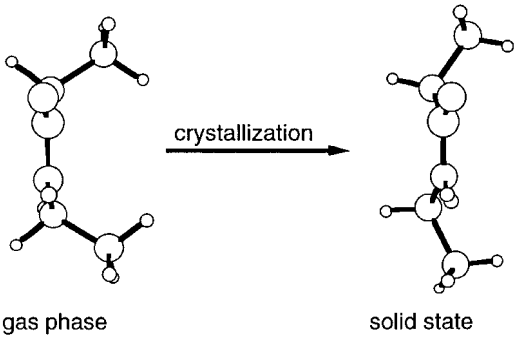

Figure 13. Conformation of *R,R*-ALADKP in the gas phase and the solid state. The DKP ring in both conformations is puckered into a boat conformation. The puckering of the DKP in the solid-state conformation is more extreme, however, in order to achieve a conformation that is more planar overall, which presumably packs more efficiently and increases the number of intermolecular interactions. Although more efficient packing is achieved, increasing the pucker of the DKP ring increases the ring strain in the molecule

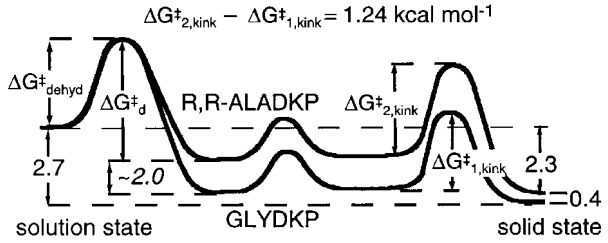

Figure 14. Energy barriers that molecules of GLYDKP and *R,R*-ALADKP must overcome during their crystallization. According to BCF theory, $\Sigma G‡$ represents the sum of the energy barriers for desolvation, surface diffusion, ledge diffusion and incorporation of solute at a kink site. The difference in free energy associated with a transition from the solution phase to the crystalline phase for *R,R*-ALADKP is 0.4 kcal mol^{-1} smaller than that of GLYDKP. $\Delta G‡_d$ is the energy barrier for desorption of a diffusing molecule of *R,R*-ALYDKP from the crystal surface, which is calculated to be ~2 kcal mol^{-1} smaller than that for GLYDKP. $\Delta G‡_{1,kink}$ and $\Delta G‡_{2,kink}$ are the respective energy barriers for incorporation of GLYDKP and *R,R*-ALADKP into a kink site, which differ by 1.24 kcal mol^{-1}

for the free energy of translation and rotation, it is reasonable to assume that the entropic changes associated with the transfer of GLYDKP and *R,R*-ALADKP from a solution state to a surface adsorbed state are also similar.[66] We estimate that the free energy of surface adsorbed *R,R*-ALADKP is ~2 kcal mol^{-1} more positive than that of GLYDKP based on our calculations (see above) of the average adsorption energies for these two compounds. Thus, in Figure 14 both solution states of GLYDKP and *R,R*-ALADKP are shown at equivalent energy levels and their surface adsorbed states are shown at energy levels separated by ~2 kcal mol^{-1}. Although the absolute energy barrier for incorporation of either cyclic dipeptide into a kink site is not known, the general activation barrier for transfer across the solution-crystal interface is typically in the range 10–25 kcal mol^{-1}.[63]

Table 1. Angles (α and γ) for the conformations of GLYDKP and *R,R*-ALADKP in the gas phase and in the solid state[a]

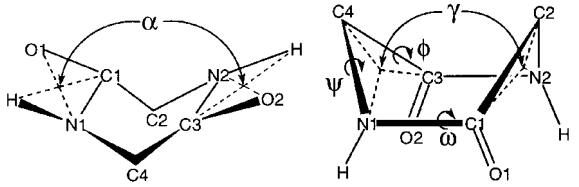

Molecule	Phase	α	γ
GLYDKP	Gas	180.0	180.0
	Solid	180.0	180.0
R,R-ALADKP	Gas	170.1	168.2
	Solid	157.4	135.7

[a] Degree of angles for α and γ were measured between the two planes (shown as an intersection of dashed lines) defined by (N1— C1— O1) and (N2— C3— O2), and (N1— C4— C3) and (N2— C2— C1), respectively.

CONCLUSIONS

Strong intermolecular interactions and molecular shape dominate the kinetics and energetics of self-assembly. To understand better the contribution of molecular shape on self-assembly, we have compared the rate at which two cyclic dipeptides assemble into supramolecular structures using atomic force microscopy as an *in situ* probe of the kinetics of step advancement in these crystalline solids. Results from these studies show that changes in the molecular structure of the substituents from two hydrogen atoms on the cyclic dipeptide of glycine (GLYDKP) to two methyl groups on the cyclic dipeptide of alanine (*R,R*-ALADKP) reduces the rate at which *R,R*-ALADKP assembles into supramolecular structures by a factor between four and five relative to that of GLYDKP. Since the barriers to desolvation for these two compounds have been reported to be similar and the barriers to surface diffusion and ledge diffusion are not rate limiting, the reduction in the kinetic coefficient of *R,R*-ALADKP relative to that of GLYDKP corresponds to a difference in the barriers to incorporation at a kink site. We calculate this difference to be 1.24 kcal mol^{-1} and suggest that the source of this difference stems from conformational changes that increase strain in the DKP ring prior to incorporation at a kink site.

Acknowledgements

G.T.R.P. is a recipient of a CAREER award from the National Science Foundation and is grateful for generous support from the NSF, ONR, DARPA, DuPont and the ACS Petroleum Research Fund.

REFERENCES

1. Demming TJ. *Adv. Mater.* 1997; **9**: 299–311.
2. Lawrence DS, Jiang T, Levett M. *Chem. Rev.* 1995; **95**: 2229–2260.
3. Rebek J. *Chem. Soc. Rev.* 1996: 255–264.
4. Paleos CM, Tsiourvas D. *Adv. Mater.* 1997; **9**: 695–710.
5. Philp D, Stoddart JF. *Angew. Chem., Int. Ed. Engl.* 1996; **35**: 1155–1196.
6. Fabbrizzi L, Poggi A. *Chem. Soc. Rev.* 1995: 197–202.
7. Desiraju GR. *Crystal Engineering: the Design of Organic Solids*, Materials Science Monographs vol. 54 Elsevier: Amsterdam, 1989.
8. Harris KDM. *Chem. Soc. Rev.* 1997; **26**: 279–289.
9. Munakata M, Wu LP, Kuroda-Sowa T. *Bull. Chem. Soc. Jpn.* 1997; **70**: 1727–1743.
10. MacDonald JC, Whitesides GM. *Chem. Rev.* 1994; **94**: 2383–2420.
11. Fan E, Vicent C, Geib SJ, Hamilton AD. *Chem. Mater.* 1994; **6**: 1113–1117.
12. Aakeröy CB, Seddon KR. *Chem. Soc. Rev.* 1993: 397–407.
13. Etter MC. *J. Phys. Chem.* 1991; **95**: 4601–4610.
14. Schmidt GMJ. *Pure Appl. Chem.* 1971; **27**: 647.
15. Kleppinger R, Lillya CP, Yang C. *J. Am. Chem. Soc.* 1997; **119**: 4097–4102.
16. Motesharei K, Ghadiri MR. *J. Am. Chem. Soc.* 1997; **1997**: 11306–11312.
17. Leiserowitz L, Schmidt GMJ. *J. Chem. Soc. A* 1969; 2372–2382.
18. Etter MC. *Acc. Chem. Res.* 1990; **23**: 120–126.
19. Etter MC, MacDonald JC, Bernstein J. *Acta Crystallogr., Sect. B* 1990; **46**: 256–262.
20. Bernstein J, Davis RE, Shimoni L, Chang N-L. *Angew. Chem., Int. Ed. Engl.* 1995; **34**: 1555–1573.
21. Leiserowitz L, Tuval M. *Acta Crystallogr., Sect. B* 1978; **34**: 1230–1247.
22. Weinstein S, Leiserowitz L. *Acta Crystallogr., Sect. B* 1980; **36**: 1406–1418.
23. Weinstein S, Leiserowitz L, Gil-Av, E. *J. Am. Chem. Soc.* 1980; **102**: 2768–2772.
24. Leiserowitz L. *Acta Crystallogr., Sect B* 1977; **33**: 2719–2733.
25. Leiserowitz L, Hagler AT. *Proc. Roy. Soc. London, Ser. A* 1983; **338**: 133–175.
26. Tokunaga Y, Rebek J Jr. *J. Am. Chem. Soc.* 1998; **120**: 66–69.
27. Bergeron RJ, Phanstiel O, Yao GW, Milstein S, Weimar WR. *J. Am. Chem. Soc.* 1994; **116**: 8479–8484.
28. Pedireddi VR, Chatterjee S, Ranganathan A, Rao CNR. *J. Am. Chem. Soc.* 1997; **119**: 10867–10868.
29. Schauer CL, Matwey E, Fowler FW, Lauher JW. *J. Am. Chem. Soc.* 1997; **119**: 10245–10246.
30. Geib SJ, Vicent C, Fan E, Hamilton AD. *Angew. Chem. Int. Ed. Engl.* 1993; **32**: 119–121.
31. Mascal M, Fallon PS, Batsanov AS, Heywood BR, Champ S, Colclough M. *J. Chem. Soc., Chem. Commun.* 1995: 805–806.
32. Lehn J-M, Mascal M, DeCian A, Fischer J. *J. Chem. Soc., Perkin Trans. 2* 1992: 461–467.
33. Zerkowski JA, MacDonald JC, Seto CT, Wierda DA, Whitesides GM. *J. Am. Chem. Soc.* 1994; **116**: 2382–2391.
34. Zerkowski JA, MacDonald JC, Whitesides GM. *Chem. Mater.* 1994; **6**: 1250–1257.
35. Schwiebert KE, Chin DN, MacDonald JC, Whitesides GM. *J. Am. Chem. Soc.* 1996; **118**: 4018–4029.
36. Lewis FD, Yang J-S, Stern CL. *J. Am. Chem. Soc.* 1996; **118**: 12029–12037.
37. Simanek EE, Tsoi A, Wang CCC, Whitesides GM, McBride MT, Palmore GTR. *Chem. Mater.* 1997; **9**: 1954–1961.
38. Palacin S, Chin DN, Simanek EE, MacDonald JC, Whitesides GM, McBride MT, Palmore GTR. *J. Am. Chem. Soc.* 1997; **119**: 11807–11816.
39. Fan E, Yang J, Geib SJ, Stoner TC, Hopkins MD, Hamilton AD. *J. Chem. Soc., Chem. Commun.* 1995: 1251–1252.
40. Mascal M, Hext NM, Warmuth R, Moore MH, Turkenburg JP. *Angew. Chem., Int. Ed. Engl.* 1996; **35**: 2204–2206.
41. Zerkowski JA, Seto CT, Whitesides GM. *J. Am. Chem. Soc.* 1992; **114**: 5473–5475.
42. Palmore GTR, McBride MT. *Chem. Commun.* 1998: 145–146.
43. Zhao X, Chang Y-L, Fowler FW, Laugher JW. *J. Am. Chem. Soc.* 1990; **112**: 6627–6634.
44. Chang Y-L, West M-A, Fowler FW, Lauher JW. *J. Am. Chem. Soc.* 1993; **115**: 5991–6000.
45. Toledo LM, Lauher JW, Fowler FW. *Chem. Mater.* 1994; **6**: 1222–1226.
46. Harris KDM, Stainton NM, Callan AM, Howie RA. *J. Mater. Chem.* 1993; **3**: 947–952.
47. Garcia-Tellado F, Geib SJ, Goswami S, Hamilton AD. *J. Am. Chem. Soc.* 1991; **113**: 9265–9269.
48. Hollingsworth MD, Santarsiero BD, Oumar-Mahamat H, Nichols CJ. *Chem. Mater.* 1991; **3**: 23–25.
49. Hollingsworth MD, Brown ME, Santarsiero BD, Huffman JC, Goss CR. *Chem. Mater.* 1994; **6**: 1227–1244.
50. Kane JJ, Liao R-F, Lauher JW, Fowler FW. *J. Am. Chem. Soc.* 1995; **117**: 12003–12004.
51. Coe S, Kane JJ, Nguyen TL, Toledo LM, Wininger E, Fowler FW, Lauher JW. *J. Am. Chem. Soc.* 1997; **119**: 86–93.
52. Aakeröy CB, Hughes DP, Nieuwenhuyzen M. *J. Am. Chem. Soc.* 1996; **118**: 10134–10140.
53. Ghadiri MR, Granja JR, Milligan RA, McRee DE, Khazanovich N. *Nature London* 1993; **366**: 324–327.
54. Khazanovich N, Granja JR, McRee DE, Milligan RA, Ghadiri MR. *J. Am. Chem. Soc.* 1994; **116**: 6011–6012.
55. Clark TD, Buehler LK, Ghadiri MR. *J. Am. Chem. Soc.* 1998; **120**: 651–656.
56. Palmore GTR, Luo TJM, McBride-Wieser MT, Picciotto EA, Reynoso-Paz CM. *Chem. Mater* 1999; **11**: 3315–3328.
57. Palmore GTR, Luo TJ, Martin TL, McBride-Wieser MT, Voong NT. *Trans. American Crystallographic Association* 1998; **33**: 45–57.
58. Weissbuch I, Addadi L, Lahav M, Leiserowitz L. *Science* 1991; **253**: 637–645.
59. Shimon LJW, Lahav M, Leiserowitz L. *Nouv. J. Chim.* 1986; **10**: 723–737.
60. Degeilh R, Marsh RE. *Acta Crystallogr.* 1956; **12**: 1007–1014.
61. Sletten E. *J. Am. Chem. Soc.* 1970; **92**: 172–177.
62. Gilmer GH, Ghez R, Cabrera N. *J. Cryst. Growth* 1971; **8**: 79–93.
63. Chernov AA. *Modern Crystallography III. Crystal Growth*. Springer: Berlin, 1984; **106**: 116–126.
64. Frank FC. *Philos. Mag.* 1951; **42**: 1014–1021.
65. Rappé AK, Goddard WA. *J. Phys. Chem.* 1991; **95**: 3358–3363.
66. Brady GP, Sharp KA. *Biophys. J.* 1997; **72**: 913–927.
67. Murphy KP, Gill SJ. *Thermochim. Acta* 1990; **172**: 11–20.